



# ATLAS NOTE

September 22, 2017



## Test of the Micromegas Trigger Processor with Cosmic Ray Muons

J. Farah<sup>a</sup>, N. Felt<sup>a</sup>, M. Franklin<sup>a</sup>, P. Giromini<sup>a</sup>, J. Phillion<sup>a</sup>, A. Tuna<sup>a</sup>, A. Wang<sup>a</sup>

<sup>a</sup>*Harvard University, Cambridge, Massachusetts 02138, USA*

### Abstract

We have commissioned a MM Trigger Processor demonstrator after adding ART Data-Driver Cards to the existing Harvard Micromegas octuplet instrumented with MMFE8 front-end boards. The MMTP spatial and time resolutions are measured using cosmic muons with energy  $\geq 0.8 \text{ GeV}/c^2$ .

Readout plane	Type	$z_{\text{board}}(\text{mm})$	$z_{\text{bary}}(\text{mm})$
0	$X$	0.0	-2.7
1	$X$	11.2	13.9
2	$U$	32.4	29.7
3	$V$	43.6	46.3
4	$U$	113.6	110.9
5	$V$	124.8	127.5
6	$X$	146.0	143.3
7	$X$	157.2	160.0

Table 1: Characteristics of the 8 Micromegas planes assembled into 2 quadruplets (see text). Planes  $x$  have electrodes parallel to the scintillator  $x$  coordinates. Electrodes of planes  $u$  and  $v$  are tilted with respect to the  $x$  electrodes by  $\pm 1.5^\circ$ , respectively. The positions along the  $z$  axis of each electrode plane are called  $z_{\text{board}}$ . The  $z$  position at half drift gap, where the barycenter is reconstructed, is called  $z_{\text{bary}}$ .

## 1 Introduction

We have implemented and debugged the firmware of the Micromegas trigger processor (MMTP) hosted momentarily in a VCT07 FPGA evaluation board. The MMTP is one of many modules contributing to the formation of the Level-1 muon end-cap trigger for the New Small Wheel (NSW) upgrade of the ATLAS muon spectrometer [1]. The MMTP uses the Address in Real Time (ART) signals issued by each VMM in the MMFE8 front-end boards and formatted by an intermediate board called the Art Data Driver Card (ADDC).

The MMTP performance is measured using our Micromegas octuplet equipped with MMFE8 front-end boards which use the VMM2 ASIC [2, 3]. Following the NSW TDR design, the ART signals are sent to the trigger processor via optical links in two steps. First, the ART signals of each board are deserialized and reformatted with 2 FPGA-based ADC V1 cards.

In these conditions, several millions of cosmic muons have been collected with the Harvard cosmic ray telescope and are used to evaluate the performance of the Micromegas trigger system reported in this note.

## 2 Cosmic muon telescope and Micromegas octuplet

The Micromegas and scintillator detectors of the Harvard cosmic ray test stand are described in detail in previous notes presenting the performance of the full MMFE8 readout [2, 3]. Eight layers of Micromegas detectors are stacked vertically for the purpose of providing eight measurements of the position of a cosmic muon as it travels through the experiment. The readout strips of each layer have a 0.4 mm pitch, and are arranged according to the NSW design:  $XXUV - UVXX$ , in which strips in the  $X$  planes run perpendicular to the readout edge of the chamber, and strips in the  $U$  ( $V$ ) planes are tilted at an angle of  $1.5^\circ$  ( $-1.5^\circ$ ) to provide a measurement of the non-precision  $y$  coordinate. Each Micromegas detector covers an active area of  $200 \times 204.6 \text{ mm}^2$ . The type and  $z$  position of the different readout planes are summarized in Table 1. Three layers of scintillators counters - placed above, on top, and below the octuplet - provide a trigger for the full MMFE8 readout. A scintillator trigger requires the coincidence of signals in all three layers. Concrete blocks, 5 feet thick, are placed between the octuplet and the bottom scintillator to harden the muon spectrum.

## 2.1 Readout electronics

The Micromegas readout electronics consists of three cards. The MMFE8 card is a demonstrator that houses 8 VMM2 ASICs per card. These ICs provide digitized arrival-time and charge information for the signal of each Micromegas readout strip. A description of the MMFE8 boards can be found in Refs. [2, 4]. A study of its performance is in Refs. [2, 3]. The MMFE8 demonstrator uses a FPGA for configuring and reading out the VMMs digitized information over ethernet. We use 8 MMFE8s to read the 512 channels of the 8 layers of Micromegas in the octuplet.

The ADDC card [1] receives data from 4 MMFE8s over miniSAS connections and packages this data into a single output for the MMTP board. For this purpose, the ADDC V1 uses a FPGA communicating with a GBTx chip. As mentioned earlier, we need two such boards.

The Micromegas Trigger Process (MMTP) is the last card of the Micromegas trigger path. It receives data from ADDCs over SFP+ optical connections and searches the data for the presence of hits consistent with a track segment using firmware running on a VC707 FPGA evaluation board. Pictures of the ADDC V1 and the demonstrator MMTP are shown in Figure 1.

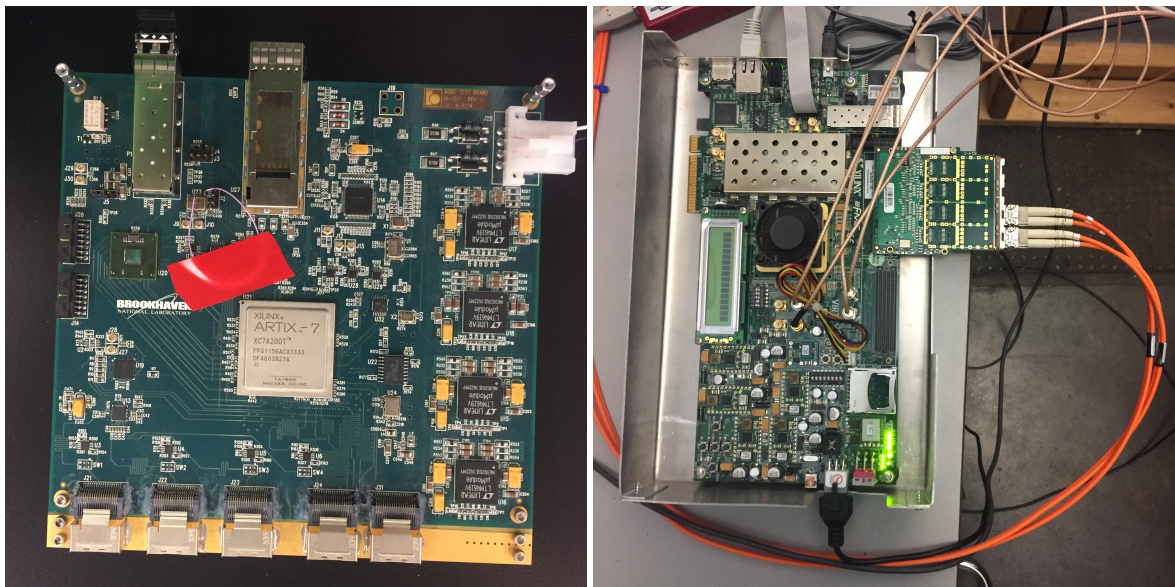


Figure 1: Pictures of the ADDC V1 (left) and the MMTP board (right).

An additional board, referred to as clock/trigger card, has been designed by J. MacArthur. This board generates and distributes a 40 MHz clock to all MMFE8 and MMTP boards. Time is measured in units of BC, where BC is a tick of this clock. The content of counters incremented using this common external clock, referred to as BCID and located in all boards, is attached to the event information. The clock/trigger cards also receive and distribute scintillator-trigger signals as discussed in Section 2.3. A flow diagram of the hardware is shown in Figure 2.

## 2.2 Trigger data path

The MMTP data path starts with the ART signal provided by each VMM. The VMM has two operating modes for the ART signal: the ART flag can be issued when the integrated charge of a signal is above threshold ( $\approx 3$  fC) or reaches its peak value ( $\approx$  chosen peaktimes, usually 200 ns). We choose the first mode to reduce the latency of the Micromegas trigger which is already quite close to the allocated 1  $\mu$ s [1].

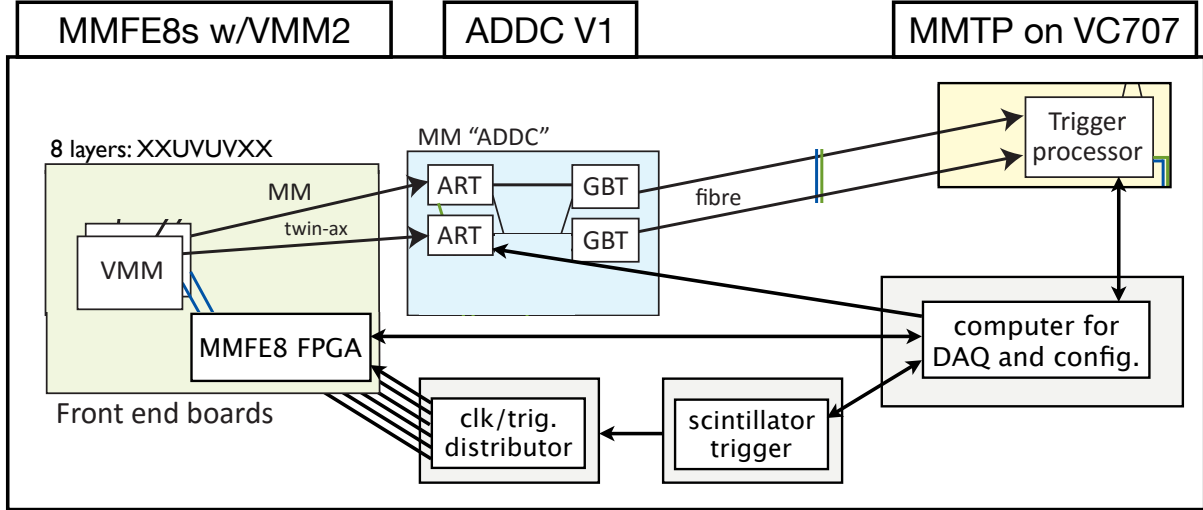


Figure 2: Schematic of the data flow in the readout electronics used at the Harvard cosmic ray test stand. Inspiration for the cartoon was provided by L. Levinson.

The ART flag is followed by the serialized address of the channel (6-bits) released at rising and falling edges of the MMFE8 160 MHz ART clock, derived by boosting up the external BC clock. At the flag falling edge, the ADDC uses the MMFE8 ART clock to deserialize the ART address. This clock, scaled down to 40 MHz, also increments a counter, the value of which at the flag is attached to the channel address together with MMFE8 board and VMM numbers (ART string). At each BC, the ADDC uses GBTx frames to collapse the ART informations of 32 VMMs into 112-bits packets which are sent through a SFP+ optical link to the MMTP board. Each frame has only space for 8 ART strings. If more strings are present, the ADDC keeps the eight with highest priority, where the priority is assigned according to the VMM position. While this is not a problem in our case, this step will need re-evaluation in the LHC high-L situation.

The e-link between each MMFE8 and the ADDC is provided by miniSAS 36-line cables in which each VMM ART output uses a preassigned pair of cables. Unfortunately, the ART clock uses pairs of unshielded sideband lines which generate quite a bit of EMI captured by the octuplet AI frame and in turn injected into the Micromegas readout electrodes. It took us a few months to discover it and one day to fix it.

The ADDC V1 were built by BNL and the firmware to receive the data, align and format them was imported by Lin Yao from the ART ASIC architecture[5]. Two mistakes were found and fixed in the firmware: a) an error in deserializing ART data with the 160 MHz clock which produced incorrect ART addresses; and b) the ART flag, variable in length, was not always detected resulting into a loss of events. Other than that, the ADDC firmware was found to be flawless. The MMTP process uses the ADDC information to find and characterize trigger candidates.

As in the NSW design, the 2 ADDCs are placed near the octuplet and the VC707 board receiving their data is placed in a 10 m away shack -elevated to control room status- which also houses the DAQ computer and scintillator trigger/readout electronics.

### 2.3 MMFE8 and scintillator data path

The ART data is distinct from the full readout of the MMFE8, as the latter includes detailed information about the charge and arrival time of all signals captured during one event. This event information is used to evaluate the MMTP efficiency, and time and spatial resolution independently of the octuplet efficiency.

The MMFE8 and scintillator data paths are described in detail in Refs. [2, 3]. Upon a scintillator trigger, the DAQ computer pulls out the MMFE8 information recorded in  $100\ \mu s$  before the trigger using an ethernet connection. The arrival time of the scintillator signals are also recorded and sent over ethernet to the DAQ computer. Micromegas and scintillator data, as well MMTP data, are recorded event by event with the DAQ-computer time stamp. This allows us to recombine the information of a single event split into different files.

The scintillator trigger, which has a 1.2 ns resolution, is also sent to the MMTP where it is stamped with content of a counter incremented by the 640 MHz clock derived from the external BC clock.

### 3 MMTP Algorithm

The MMTP algorithm is described in detail in Refs. [6, 7]. The trigger algorithm is summarized here, mostly to describe the adjustments made to utilize the algorithm with a cosmic muon detector.

The MMTP algorithm receives ADDC data and converts the ART addresses into Cartesian coordinates, look for subsets (“triggers”) which satisfy spatial and time prerequisites, and calculate quantities which characterize these triggers. The first step is referred to as the *decoder*, the second step is referred to as the *finder*, and the third step is referred to as the *fitter*. The present MMTP is firmware is synthesized and run on a Xilinx Virtex-7 FPGA in a VC707 evaluation board.

#### 3.1 Decoding

The MMTP converts the VMM and strip numbers into Cartesian coordinates, rotated with respect to each other by the stereo angle for  $X$ ,  $U$ , and  $V$  planes, and taking into consideration that some of the MM chambers are flipped relative to each other.

The MMTP measures coordinates in units of strip pitch ( $400\ \mu m$ ). For example, if strip 30 in VMM 5 is converted into a position  $x = 350 = 5 * 64 + 30$ . For each board, the algorithm uses the  $z$ -locations listed in Table 1.

#### 3.2 Finder

The next step of the MMTP algorithm is to search the data of all boards (at different  $z$  positions) for hits in given time window and  $x$  road. The finder assigns hits in each board to a number of  $x$ -roads, and evaluates simultaneously if any road contains enough hits to generate a trigger. Because our telescope accepts track with angle of incidence between  $-10^\circ$  and  $25^\circ$ , the algorithm uses  $x$ -roads 1 VMM wide (1 VMM corresponds to 64 strips and 25.4 mm).

A road must contain at least two hits on the  $X$  planes and at least two hits on the stereo ( $UV$ ) planes to generate a trigger. Additionally, at least two of the hits on  $X$  planes must occur on different quadruplets, to ensure a good slope resolution when later fitting the  $X$  hits with a straight line.

Taking advantage of the low rate of ART signals, we use requirements looser than those ( $3X$  and  $3UV$ ) anticipated in the NSW TDR to compensate for the MMFE8 board inefficiencies caused by the increasing number of VMM channels zapped by the Micromegas high voltage [3]. A graphic visualisation of the finder algorithm is shown in Fig. 3. To recover those cases in which a muon with a large angle of incidence deposits hits in two different roads, the finder algorithm also searches for hits in the 2 neighboring roads. For example, road 3 uses hits from VMM 2, VMM 3, and VMM 4, so that the effective road size is 3 VMMs.

The finder also requires candidate hits to lie within a given time window in units of the BC clock.

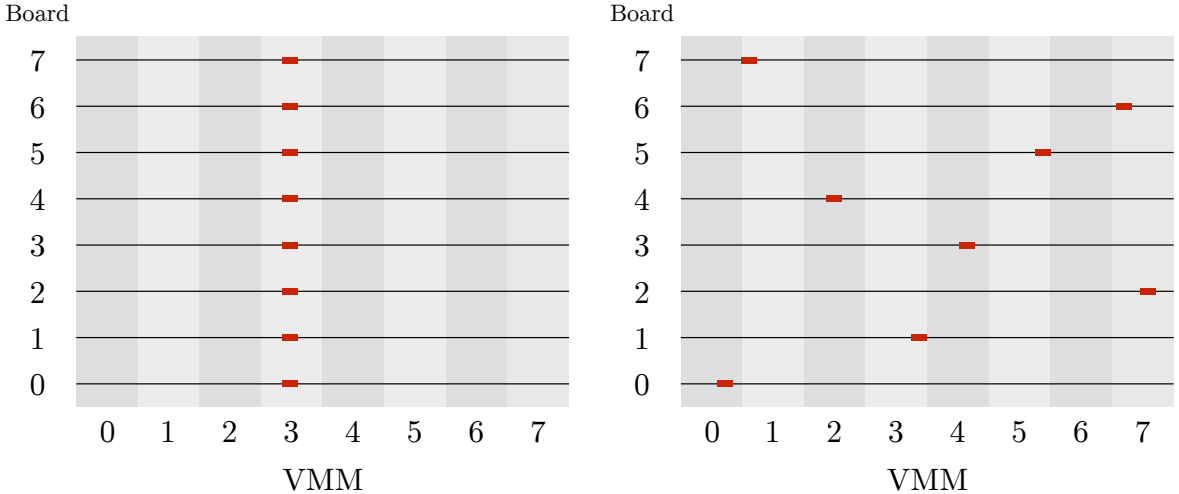


Figure 3: Hits generated by a cosmic muon passing through the octuplet (left) and randomly generated (right) as seen by the finder algorithm. Roads are 1-VMM wide and shown in alternating gray colors. Only the event on the left will generate a trigger.

Based on previous measurements of the time jitter of ART signal [8], we choose a 8 BC window<sup>1</sup>. The time window is implemented as follows. A board hit in a given road is stored for 8 BCs. No new hits are allowed in that road for that board until the hit is “old”, i.e., after eight BCs. As new hits are entering into other boards in the same road, the trigger requirements are evaluated at every BC. Triggers are searched for in all roads simultaneously. If a trigger is found in a road, a trigger is issued when the earliest hit in the road becomes “old”. That trigger will carry the BCID of the “old” hit.

Each road can provide one trigger per cycle of the BC clock. The triggers found in all roads with the same BCID are placed in a road-number-based priority encoder and sent sequentially to the fitter for further calculations. Because the MMTP clock is eight times faster than the BC clock, the fitter can process close to 8 triggers. In our case, no found trigger is lost.

### 3.3 Fitter

The *fitter* algorithm provides the location and quality of a trigger. The location is represented by a point in the  $\eta - \phi$  space which in the NSW upgrade is used by downstream trigger modules to define the L1 muon trigger region of interest (ROI).

In ATLAS, the global slopes are calculated as  $m_l = < x_l / z_l >$ . For each hit in  $l = X$  or  $l = U$  or  $l = V$  planes, the quantity  $x_l / z_l$ , where  $x_l$  is the coordinate value and  $z_l$  is the distance from the interaction point ( $\approx 750$  cm), is returned by look-up-tables (LUT). Averages are calculated by the fitter algorithm. The 3 slopes are converted with look up tables which return  $m_y = \frac{m_U - m_V}{2 \tan(\theta_{\text{stereo}})}$  and  $\eta, \phi$  coordinates from the  $m_x, m_y$  values.

In parallel, the algorithm also fits all hits in the  $X$ -planes with a straight line returning a local slope  $m_x^l$ . A cut on the slope difference  $\Delta\theta = |\theta_g - \theta_l|$ , the angles derived from the  $m_x$  and  $m_x^l$  slopes, is supposed to be used to reduce the rate of accidental triggers

Since cosmic muons do not originate from a point-like source, the fitter algorithm has been modified to use strip numbers instead of slopes (we use a new LUT which does not divide  $x$  by the distance from the interaction point). The local slope is evaluated as  $m_x^{\text{local}} = \sum c_i x_i$ , where the sum includes all  $X$  hits,

<sup>1</sup>Due to a timing bug in the MMTP firmware, this window in Run 3522 is usually 7 and seldom 8 BCs. The bug was corrected prior to Runs 3527-3530. Runs are discussed in more detail in Section 4.

and  $c_i$  are constants, stored in a new LUT, which depend on the  $z$  position of the  $X$  plane (see Table 1) in units of strip pitch. The detector distance from the beamline is set to 0. Instead of the global slope, the algorithm evaluates  $\langle x_l \rangle$  and  $\langle z_l \rangle$  for  $l = X, U, V$  hits separately.

Once a trigger has been processed, our algorithm stores: a) the ADDC data in 15 BC preceding the trigger BCID; b) the trigger BCID, the address of the hits providing a trigger, the local slope, and other ancillary information; and c) the BCID of a scintillator trigger into 3 different FIFO, the content of which is transmitted as UDP packets in round-robin mode and recorded.

### 3.4 Method for evaluating the MMTP performance

We check the MMTP performance by using events in which we can reconstruct a track using Micromegas clusters. The cluster selection is described in Ref. [2]. In particular, the BCID of the hits forming a cluster is required to be in a 15 BC window around the BCID of the scintillator trigger. As explained in Ref. [2], we fit the available cluster with two straight lines in the  $x - z$  and  $y - z$  planes. The fits, referred to as MM fits, are performed in the same coordinate system as the MMTP. The fits provide slopes,  $M_X$  and  $M_Y$ , and intercepts,  $A_X$  and  $A_Y$ , which are used to set limits to the MMTP space resolution. In the fair assumption that the uncertainty of the parameters returned by the MM fits are negligible, comparisons with MMTP results measure its accuracy.

We select tracks the clusters of which satisfy the trigger requirements. The number of MMTP triggers found in the latter set measures the MMTP efficiency.

To measure the angular resolution we compare the MMTP  $\langle x_X \rangle$  to  $A_X + M_X \langle z_X \rangle$ . The rms value of this difference, referred to as  $x_{\text{TP}} - x_{\text{MM}}$ , when divided by 750 cm, yields the  $m_x$  resolution.

We also evaluate the MMTP accuracy in measuring the  $y$  coordinate. We extrapolate the MMTP  $\langle x_U \rangle, \langle x_V \rangle, \langle x_V \rangle$  values to a common  $z_c$  value using the slope value returned by the MM fit. At that  $z_c$ , we evaluate  $y_{\text{TP}}$  as  $\frac{x_U - x_V}{2 \tan(\theta_{\text{stereo}})}$  or  $\frac{x_X - x_V(U)}{\tan(\theta_{\text{stereo}})}$  or  $\frac{x_X - x_V(V)}{\tan(\theta_{\text{stereo}})}$  (we average the various values). We then compare  $y_{\text{TP}}$  to  $y_{\text{MM}}$  derived from the MM fit at the same  $z$ . The rms value of distribution of their difference divided by the detector strip length is suggestive of the achievable  $\phi$  segmentation.

The distribution of the difference between angles corresponding to the slope of the MMTP local fit and that corresponding to  $M_x$ , referred to as  $\theta_{\text{local}} - \theta_{\text{MM}}$ , provides a measure of the resolution of the MMTP local fit.

## 4 Data taking

The data described in this note were collected from May 2017 until July 2017. Each continuous period of data-taking is referred to as a “run”, and the runs are listed in Table 2. One notes that here are many more MMTP events than MMFE8 events. There are several reasons for this. The MMTP sends data whenever the finder finds a trigger, whereas the MMFE8 only sends data only when it receives a trigger signal from the scintillator (the scintillator trigger rate is about 1 Hz rate, and 60% of the triggers contain a good track with 4 or more clusters and triggerable).

For a good track, the MMTP typically produces a handful of triggers due to the overlapping roads. For example, a downward-going muon passing entirely through road 2 also generates triggers in roads 1 and 3. In addition, if a track has more hits than the minimum required by the finder, when some of these hits get old additional triggers can be produced. A large number of triggers can be also produced by non-random noise. This seems to be the case for run 3522 and 3530. This started a long investigation of the noise source. The cause has been now identified as EMI produced by the ART clock transmitted from the MMFE8 to the ADDC through an unshielded pairs of wires in the miniSAS cable and by the AC/DC converter powering the ADDC.

Between Runs 3522 and 3527, two front-end cards were repaired and replaced on the detector. Therefore, only data from Runs 3527, 3528, and 3530 are used to compare the MMTP performance using different peaktimes in Sec. 5.4

Run	Dates	MMFE8 Events	MMTP Events	Notes
3522	05/11 - 05/18	296532	15774567	200 ns integration time
3527	06/26 - 07/02	233645	3635093	100 ns integration time
3528	07/02 - 07/07	205053	3253330	50 ns integration time
3530	07/19 - 07/24	192114	4060891	200 ns integration time

Table 2: Run information.

## 4.1 Combining data streams

As already mentioned, five data streams are produced and recorded on disk. In addition to the scintillator and MMFE8 data streams, the MMTP algorithm writes a data stream (TPFIT) with the trigger properties - including its BCID as explained earlier, a data stream (GBT) with ADDC data in the 15 the BC preceding the MMTP trigger, and a data stream (SCTBC) containing the the scintillator trigger time converted into a 16-bit BCID.

Scintillator data, MMFE8 data, and SCTBC data are easily combined (SC+MM data) using the event number and occasionally the DAQ time stamp. Because the MMTP rate is much higher, we combine it with SC+MM data through several steps: a) we select SC+MM data which contain MM clusters compatible with a track and which also satisfy the MMTP finder; d) we select TPFIT events first with a DAQ time stamp within 100 ms from that of the SC+MM event and then in a 3 BC window around SCTBC; c) of the remaining events in the TPFIT data, we pick the one which has more VMMs and boards in common with the MM clusters.

To associate GBT events to TPFIT events, we use the event number and BCID comparisons between BCID trigger and ADDC hits.

## 5 MMTP Performance

We follow the method outlined in Sec. 3.4 which uses a well reconstructed track which should provide a MMTP trigger. Figure 4 shows the efficiency of the MMTP algorithm and the number of hits generating a trigger as a function of time. In Fig. 5, we compare the distribution of the muon angles of incidence as measured by the MMTP and offline using MMFE8 clusters, as well as the number of MMTP hits and MMFE8 clusters used to reconstruct a muon track. As discussed in Sec. 3.2, the  $\simeq 0.3\%$  inefficiencies of the MMTP are due to the 8 BC window used by the finder.

### 5.1 Offline roads

In order to cover the angular acceptance of our telescope, the MMTP algorithm uses 1 VMM roads, and effectively 3 VMM roads after including neighboring roads. Because the rate of ART noise signals issued by each VMM ranges between 100 and 300 Hz, in our case accidentals triggers or accidental hits replacing good hits of a track are not an issue. In our case, the spatial resolution is largely degraded by  $\delta$  rays with energies as low as a few KeV, which in  $\simeq 15\%$  of the events replace a correct ART hit (see Fig. 6).

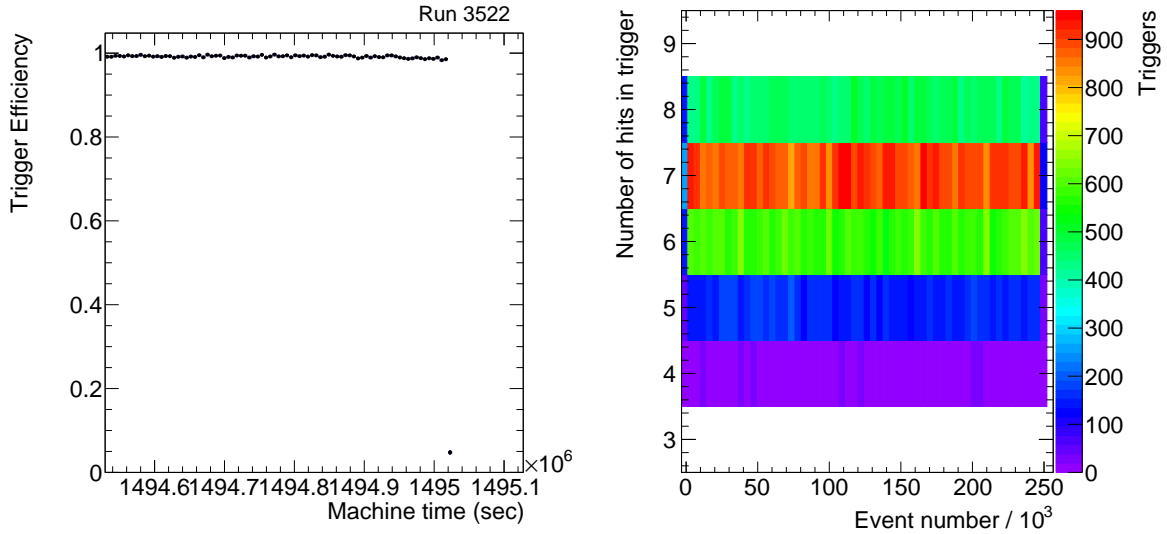


Figure 4: MMTP efficiency (left) and the number of hits producing a trigger (right) as a function of time.

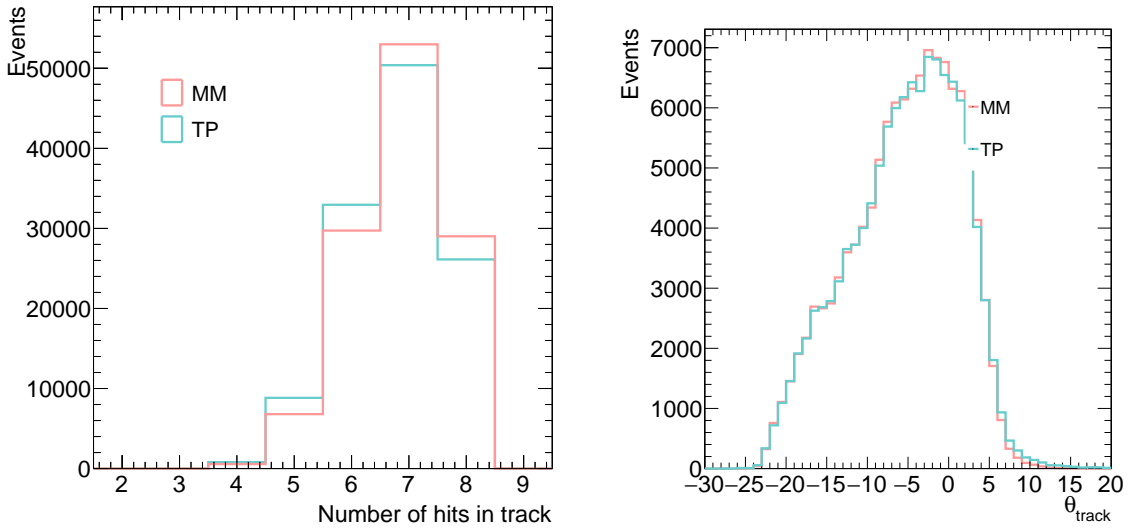


Figure 5: Distribution of the number of hits and clusters in the MMTP and MM reconstructed tracks (left). Distribution of the track's angle reconstructed by the MMTP and offline using MM clusters (right).

As the material in front of the NSW detector cannot be less than that in front of our octuplet,  $\delta$  rays will represent an irreducible source of performance degradation. Of course, this effect is reduced when using smaller roads as is the case for the NSW algorithm which plans to use 0.9 mr roads for  $X$  planes, corresponding to 1/4 VMM roads for our algorithm.

For stereo planes, the NSW road size depends on the length of the Micromegas  $x$  strips which ranges from 500 to 2200 cm as shown in Fig. 7. For the shortest and longest readout strips, stereo roads need additional 13 mm (or 32 strips) and 58 mm (144 strips) to cover just one  $x$  strip, respectively. In the following, we first show resolutions using 1 VMM roads with neighbor roads. Then, we emulate the NSW roads using the track direction provided by fitting MM cluster. For  $X$  planes, the offline finder uses

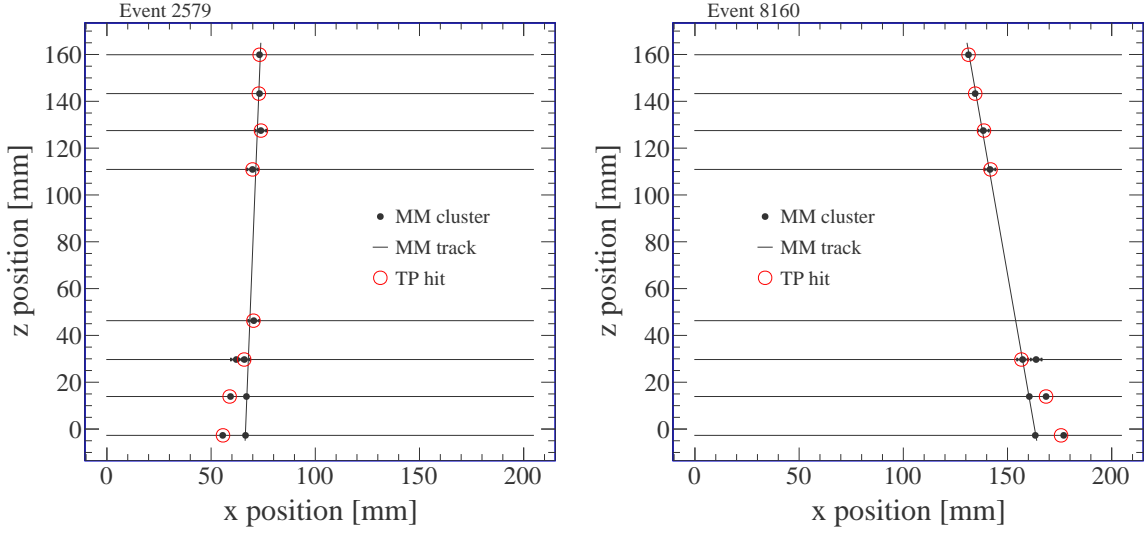


Figure 6: Display of two events with  $\delta$  rays. The black points are MM clusters, the black line is the fit to the clusters, and the red circles are the hits chosen by the MMTP. We select these events by requiring that the difference between the  $\theta$  angles reconstructed by the MMTP and offline using MM cluster is larger than 10 mr.

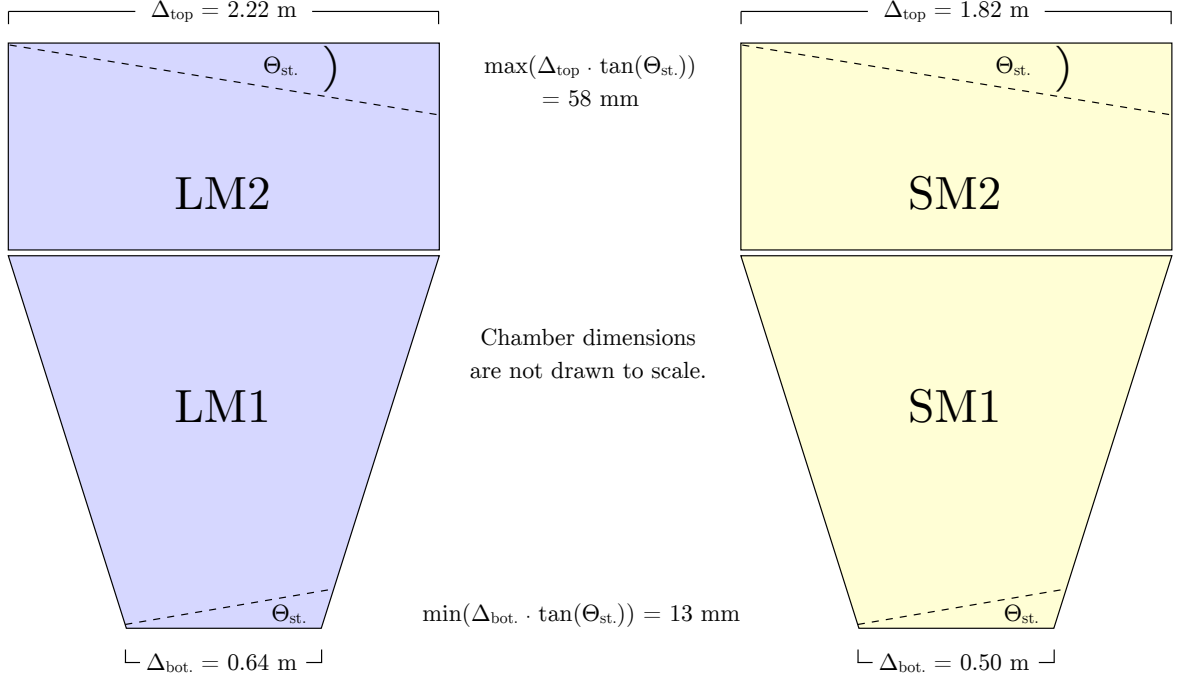


Figure 7: Drawings of Micromegas wedges with dimensions as specified by the NSW TDR. The stereo strips require larger roads than the horizontal strips because they overlap a band of  $x$  strips of width from 13 to 58 mm.

only ART hits which are at a distance of  $\pm 24$  strips from the intersection of the track with the plane (three 1/4 VMM roads). For  $U, V$  planes, the road is increased by 32 up to 144 strips. The latter increase brings the road width back to the 3 VMMs required online. These X and stereo roads emulating the NSW algorithm will be referred to as XNSW, SNSW, LNSW in the following.

## 5.2 Spatial and angular resolution

Figures 8 to 9 show the  $x_{\text{TP}} - x_{\text{MM}}$  and  $y_{\text{TP}} - y_{\text{MM}}$  distributions derived with the method in Sec. 3.4, respectively.

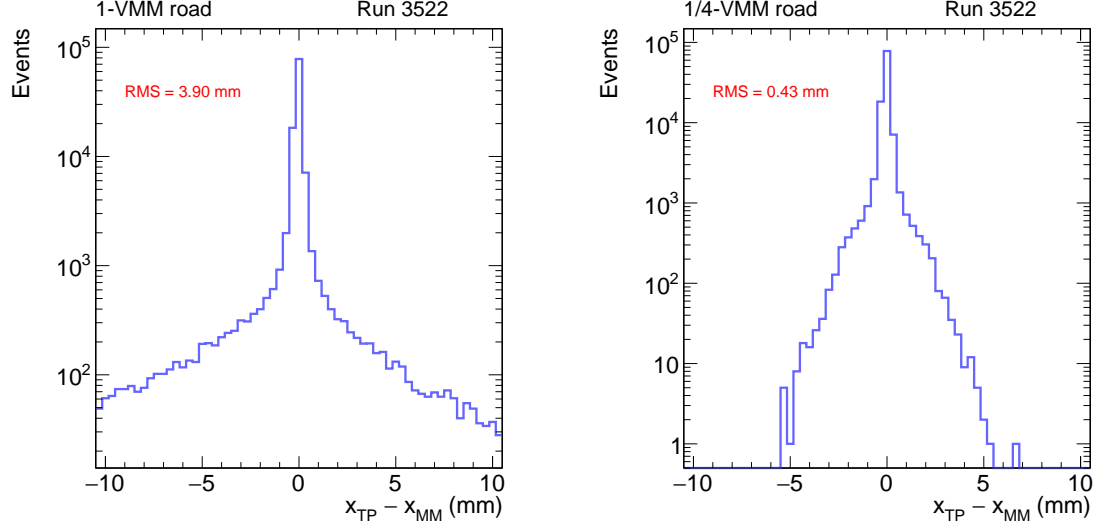


Figure 8: Distributions of  $x_{\text{TP}} - x_{\text{MM}}$  using (left) 1 VMM roads and (right) XNSW roads (see text).

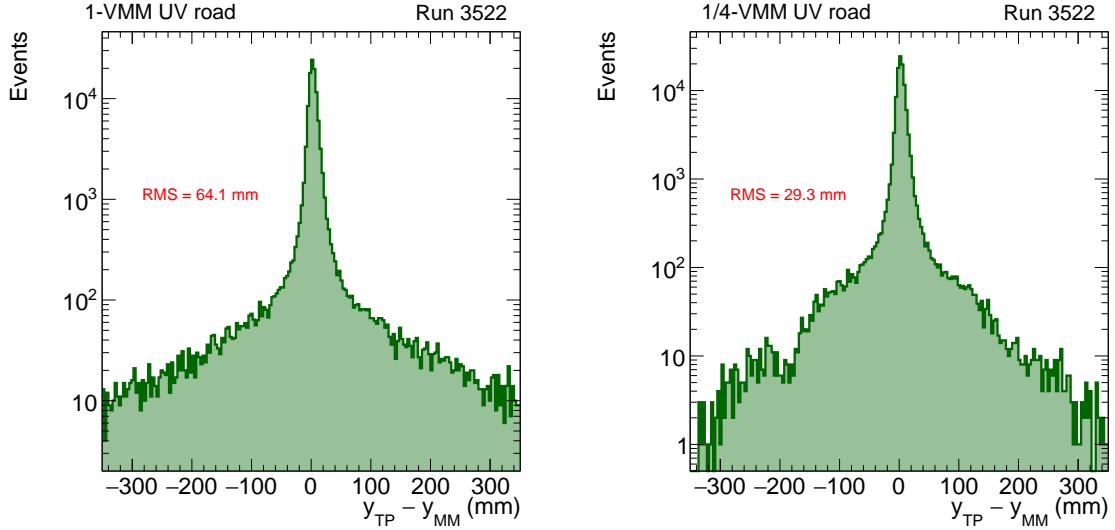


Figure 9: Distributions of  $y_{\text{TP}} - y_{\text{MM}}$  using (left) 1 VMM or LNSW roads and (right) SNSW roads (see text).

As expected, the large tails of the above distribution shrink with the road width. The global angle resolution  $0.43 \text{ mm}/7.5 \text{ m} = 0.06 \text{ mr}$  is better than what required by the NSW TDR. The  $y$  resolution segments at  $\pm 1\sigma$  level the shortest SM1 detector into 8  $\phi$  sectors and the longest LM2 detector into 17  $\phi$  sectors.

The distribution of  $\theta_{\text{local}} - \theta_{\text{MM}}$  is plotted in Fig. 10. The correlation between angular and spatial resolution is shown by Fig. 11. The NSW TDR calls for a 15 mr cut on the difference between the global and local angles. Because of  $\delta$  rays, this cut loses at least 4% of good triggers. At the highest LHC luminosities, the rate per Micromegas strip is anticipated to be as large as 50 kHz per strip, almost independent on the distance from the beamline. It seems plausible that accidental hits due to single rates will cause an even higher inefficiency of the MMTP trigger if the  $\Delta\theta$  cut is implemented.

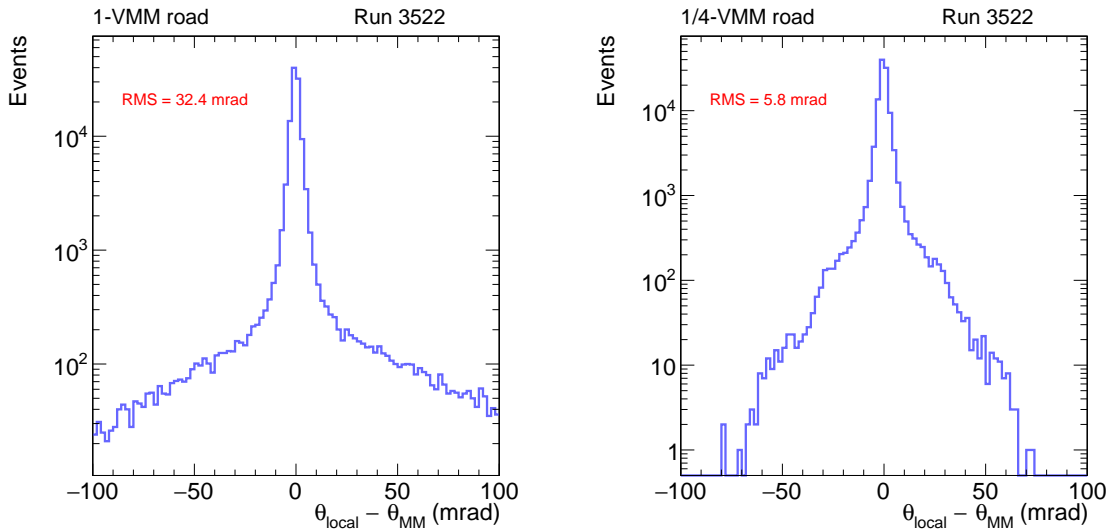


Figure 10: Distribution of  $\theta_{\text{local}} - \theta_{\text{MM}}$  using (left) 1VMM and (right) XNSW roads (see text).

### 5.3 Time resolution

Based on a previous study of ours and prudence, the MMTP algorithm makes use of a 8 BC window to form a trigger. Figure 12 shows the distribution of the number of BC clocks used by the algorithm to find a trigger for all events using a 200 ns peaktimes. If all hits arrive at the same BC, the BC window is 1. The necessity of a larger window follows from the time jitter of the individual ART signals which can be better measured by the distribution of the BC difference between any two ART signal forming a trigger (shown also in the same figure). The time distribution of ART signals is fairly well described by a Gaussian function with a  $\sigma$  of 40 ns.

The precise measurement of the trigger BCID is needed to match tracks found in the NSW with tracks found by the TGCs in the big wheel. We use two methods to define the trigger BCID: the average of the BCID of all hits and the BCID of the earliest hit. As shown in Fig. 13, the resolution is approximately 1 BC.

### 5.4 Peaktimes dependence

It is a urban legend that the time-jitter of the ART signal generated at threshold is dominated by the variation of the signal amplitude. In Ref. [8], we did show that the time jitter is mildly affected by this cause. In the following, we check this again using 200 ns, 100 ns, and 50 ns peaktimes.

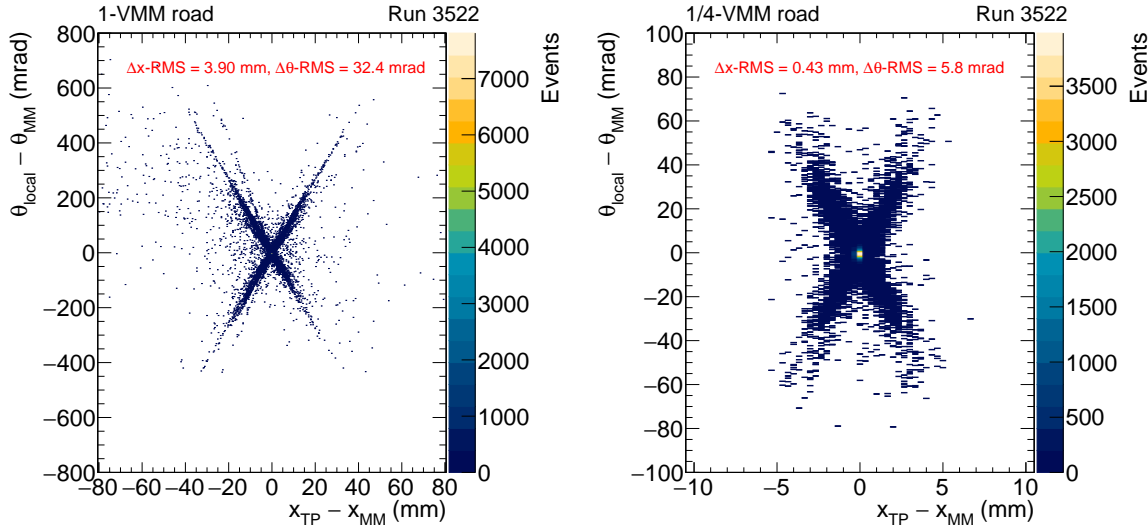


Figure 11: 2D plots of  $\theta_{local} - \theta_{MM}$  vs  $x_{TP} - x_{MM}$  using 1-VMM online roads (left) and 1/4-VMM offline roads (right), as discussed in Section 5.1. The tails of the resolution are greatly suppressed with smaller roads.

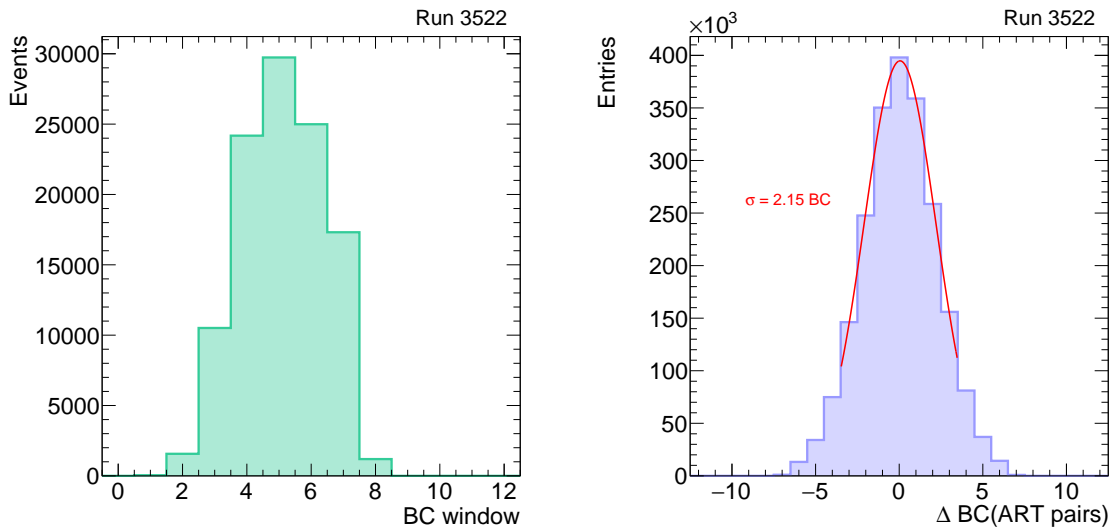


Figure 12: Distribution of the BC window used to produced a trigger for all events (left); Distribution of the BC difference of all pairs of ART signals forming a trigger (right). The data are well described by a Gaussian function. The  $\sigma$  written in the plot is the result of the fit to this distribution.

We run our detector at very high voltage and gain. The detector efficiency is little affected by the chosen peaktimes. The cluster multiplicity decreases by  $\simeq 5\%$  when halving the peaktimes.

The time distributions, analogous to those in Fig. 12 to 13 are shown in Fig. 14 to 17. The time distribution of individual ART follows is Gaussian function with  $\sigma$  decreasing from 40 ns to 32 ns when reducing the peaktime from 200 ns to 50 ns.

We use a Monte Carlo simulation to evaluate the efficiency of the MMTP algorithm as a function of

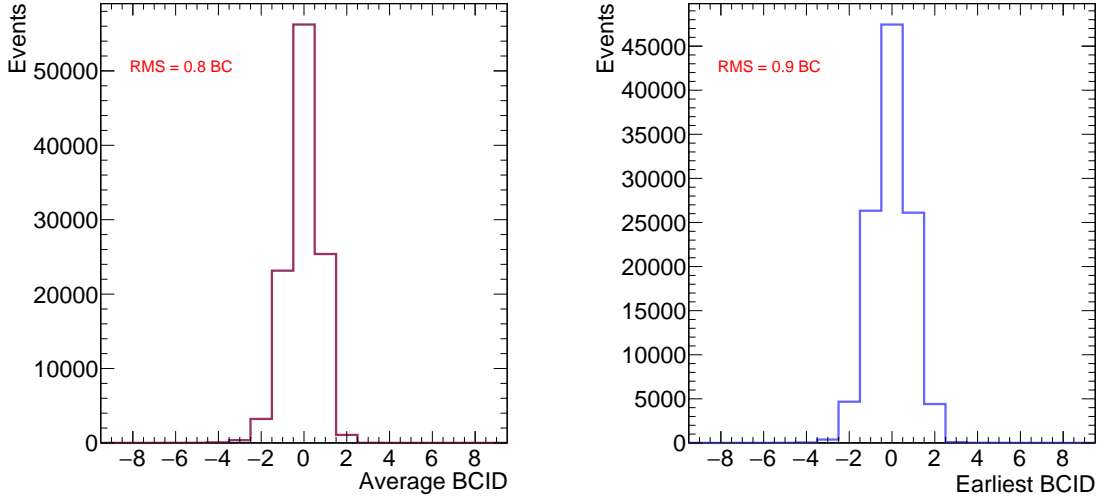


Figure 13: Distributions of the BCID difference between the scintillator trigger and the MMTP trigger. The scintillator trigger has a time resolution of 0.05 BCID.

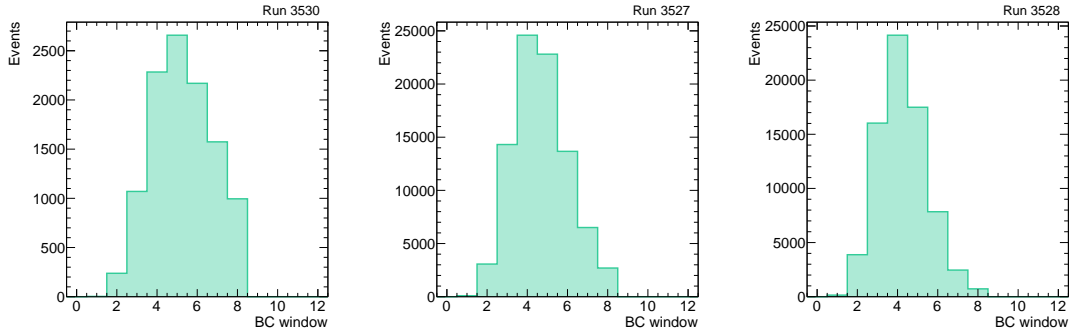


Figure 14: Distribution of the BC window used to produced a trigger for all events collected with (left) 200, (center) 100, and (right) 50 ns peaktme.

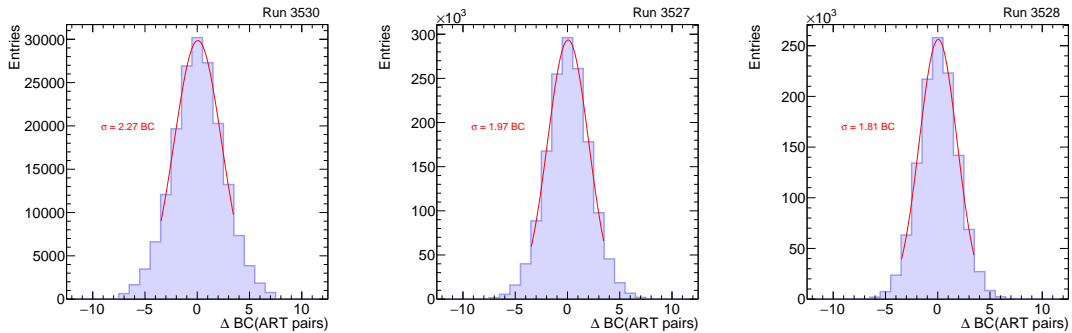


Figure 15: Distribution of the BC difference of all pairs of ART signals forming a trigger for all events collected with (left) 200, (center) 100, and (right) 50 ns peaktme. The data are well described by a Gaussian function. The  $\sigma$  written in the plot is the result of the fit to this distribution.

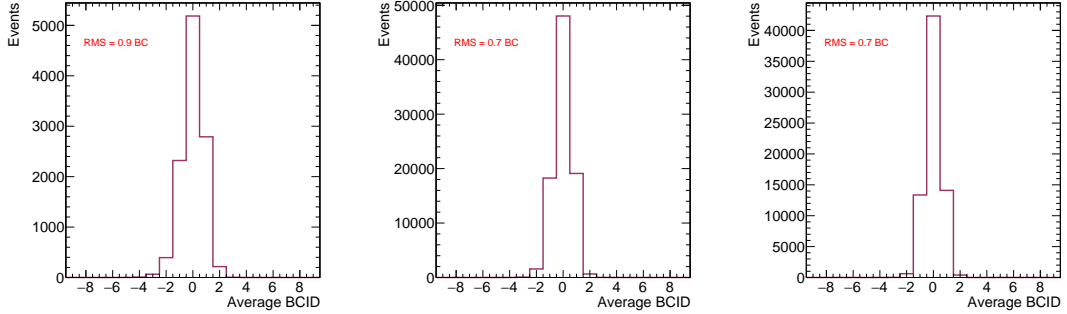


Figure 16: Distributions of the BCID difference between the scintillator trigger and the MMTP trigger for all events collected with (left) 200, (center) 100, and (right) 50 ns peaktme. The MMTP time is evaluated as as the average BCID of the ART hits.

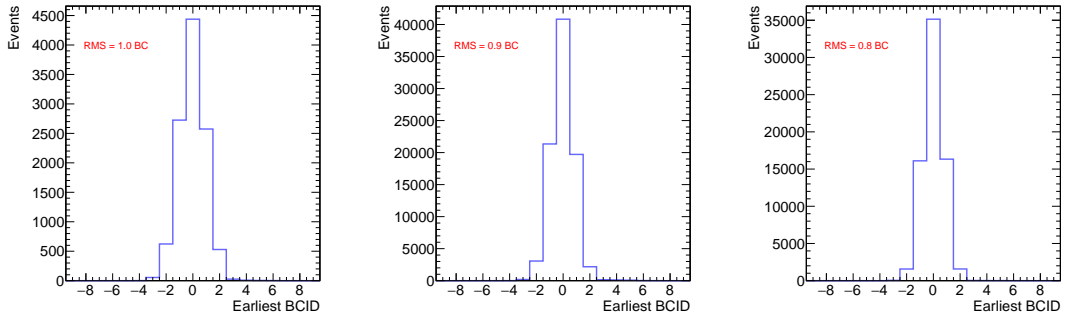


Figure 17: Distributions of the BCID difference between the scintillator trigger and the MMTP trigger for all events collected with (left) 200, (center) 100, and (right) 50 ns peaktme. The MMTP time is evaluated as as the BCID of the earliest ART hit.

the BC window for different peaktme. The result is shown in Fig. 18.

## 6 Conclusion

Using millions of cosmic tracks, we have commissioned a prototype of Micromegas trigger processor, and measured its performance using tracks reconstructed with Micromegas clusters. We use trigger roads as large as 1 VMM, and offline we reduce them to 1/4 VMM to evaluate the NSW performance.

In this condition,

- a) the  $\theta_{\text{global}}$  accuracy is found to be 0.06 mrad, better than what is needed;
- b) the  $\theta_{\text{local}}$  accuracy is spoiled by  $\delta$  rays. A 15 mrad cut on the difference of these two angles reduces the MMTP efficiency by 4%;
- c) we did not measure directly the MMTP  $\phi$  resolution. From the accuracy in measuring the non-precision coordinate, we estimate that the MMTP  $\phi$  resolution is 33 and 14 mrad for the shortest (which are closest to the beam line) and longest Micromegas readout strips, respectively.

Considering that a NSW module will hardly reach a 100% efficiency, it seems prudent to start accepting that the MMTP algorithm will need to use a 7-8 BC window, independent of the VMM peaktme.

In our measurements, the rate of uncorrelated noise is about 2 Hz per strip. Using a large BC window, the MMTP spatial accuracy will be further degraded by accidental hits at the highest LHC planned

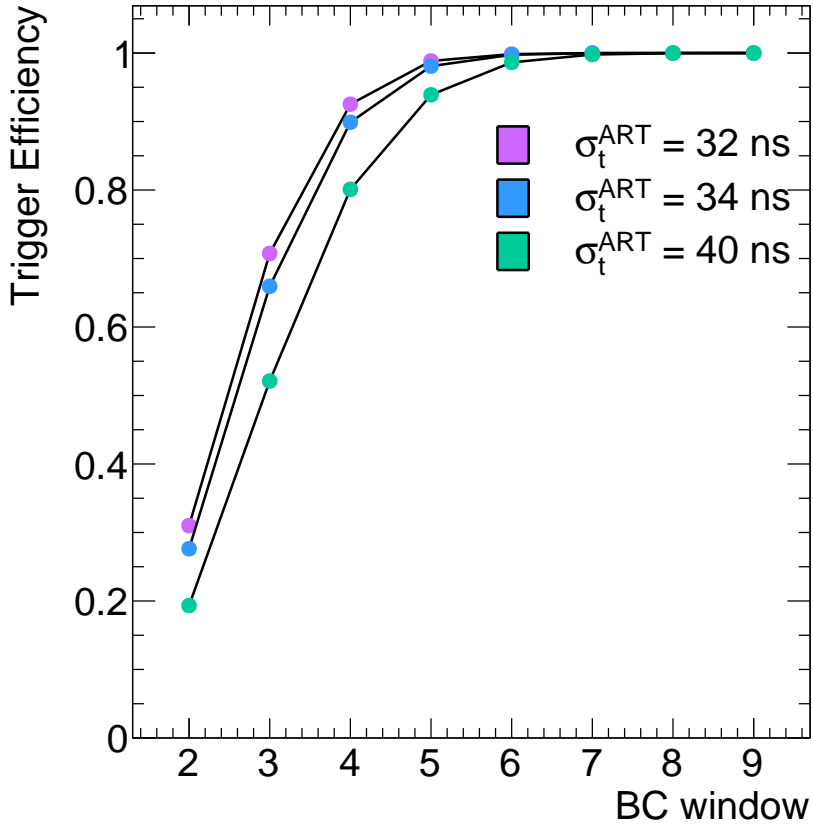


Figure 18: Simulated efficiency of the MMTP algorithm as a function of the BC window for different peaktimes. This estimate is based on an octuplet with 100% efficiency.

luminosity. One expects a rate of about 40 kHz per strip, almost independent of the distance from the beamline.

We are presently simulating the MMTP response in this high background environment. In particular, we are investigating the use of  $\leq 1/8$  VMM roads for forming triggers. Such narrow roads might not require the use of local fits to reduce the background, thus eliminating the bottle-neck of the fitter (only a few found triggers can be fitted at each BC) and also reducing the trigger latency.

## References

- [1] ATLAS New Small Wheel Technical Design Report. [ATLAS-TDR-020](#).  
[ATL-COM-MUON-2017-036](#).
- [2] P. Giromini *et al*, Performance of a Micromegs octuplet in the time of noise.  
[ATL-COM-MUON-2017-036](#).
- [3] P. Giromini *et al*, Performance of a Micromegs octuplet after removing the major cause of noise.  
[ATL-COM-MUON-2017-040](#).
- [4] <https://twiki.cern.ch/twiki/bin/viewauth/Atlas/NewSmallWheel>.
- [5] [https://twiki.cern.ch/twiki/pub/Atlas/February\\_2015\\_design\\_reviews/ADDC\\_document\\_for\\_2015\\_Feb\\_NSW\\_review\\_v1.0.pdf](https://twiki.cern.ch/twiki/pub/Atlas/February_2015_design_reviews/ADDC_document_for_2015_Feb_NSW_review_v1.0.pdf).
- [6] B. Clark *et al*, An Algorithm for Micromegas Segment Reconstruction in the Level-1 Trigger of the New Small Wheel. [ATL-COM-UPGRADE-2014-012](#).
- [7] S. Chan et. al. Micromegas Trigger Processor Algorithm Performance in Nominal, Misaligned, and Misalignment Corrected Conditions. [ATL-COM-UPGRADE-2015-033](#).
- [8] K. DiPetrillo it et al, ATL-COM-MUON-2014-069.
- [9] Simulation of the ATLAS New Small Wheel (NSW) System [ATL-MUON-SLIDE-2017-248](#).